Available online at www.sciencedirect.com
SCIENCE DIRECT®
Journal of Molecular Spectroscopy 223 (2004) 20–30
Journal of MOLECULAR SPECTROSCOPY
www.elsevier.com/locate/jms

The far-infrared laser magnetic resonance spectrum of the ^{13}CH radical

Stephen A. Davidson,[a,1] Kenneth M. Evenson,[a,2] and John M. Brown[b,*]

[a] *Time and Frequency Division, NIST, 325 Broadway, Boulder, CO 80303, USA*
[b] *The Physical and Theoretical Chemistry Laboratory, South Parks Road, Oxford OX1 3QZ, UK*

Received 9 July 2003; in revised form 18 August 2003

Abstract

Transitions between the spin-rotational levels of the ^{13}CH radical in the $v = 0$ level of the $X^2\Pi$ ground state have been detected by the technique of laser magnetic resonance at far-infrared wavelengths. These measurements have been combined with the previous measurements of the lambda-doubling intervals of the molecule [J. Chem. Phys. 85 (1986) 1276] to determine an improved set of molecular parameters for ^{13}CH. The analysis provides accurate predictions of the transition frequencies between the low-lying spin-rotational levels of the radical at zero magnetic field. A comparison is made with the values of the corresponding parameters of ^{12}CH which reveals small effects due to the breakdown of the Born–Oppenheimer approximation.

1. Introduction

The CH radical plays an important part in many chemical processes, both terrestrial and astrophysical. Consequently, there is a strong incentive to characterise the molecule in as many of its isotopic modifications as possible. Although the principal properties of the dominant isotopomer ^{12}CH have been known for a long time [1], the most detailed information on the molecule in its ground state has been gathered quite recently [2–6]. The deuterated form, CD, is also well characterised from studies of its optical [7], infrared [8,9] and far-infrared spectra [10]. However, our knowledge of the third isotopomer, ^{13}CH, is comparatively limited. Following the identification of some lines in its solar spectrum [11] (see also [12]), there have been detailed studies in recent years of the $A^2\Delta$–$X^2\Pi$ [13], the $B^2\Sigma^-$–$X^2\Pi$ [14] and the $C^2\Sigma^+$–$X^2\Pi$ transitions [15] at rotational resolution. Steimle et al. have measured the lambda-type doubling intervals in the $X^2\Pi$ state by microwave-optical double resonance [16,17]. Two ab initio calculations on ^{13}CH also exist [18,19].

In this paper, we report a study of ^{13}CH in the $v = 0$ level of the $X^2\Pi$ ground state by far-infrared laser magnetic resonance (LMR). This provides the most accurate measurement of all the major molecular parameters to date. It is in effect a companion study to those of ^{12}CH and CD by far-infrared LMR [3,10] and, as such, makes an interesting comparison with them.

2. Experimental details

The far-infrared LMR experiments were performed at the Boulder laboratories of NIST as in the earlier work on ^{12}CH [3] and CD [10]; the spectrometer has been described in detail elsewhere [20]. The ^{13}CH radicals were produced in the spectrometer sample volume by the reaction of fluorine atoms with $^{13}CH_4$ in a flow system, the fluorine atoms being generated by passing a mixture of 10% F_2 in helium through a microwave discharge. The total pressure in the sample volume was between 0.13 and 0.26 mbar (13–26 Pa) which permitted Lamb dips to be observed on most of the strong lines. Somewhat stronger ^{13}CH signals could be obtained from the reaction between F atoms and $^{13}CH_3OH$ but

* Corresponding author. Fax: 1-44-1865-275410.
E-mail address: jmb@physchem.ox.ac.uk (J.M. Brown).
[1] Present address: MIT Lincoln Laboratory, 244 Wood Street, Lexington, MA 02420, USA.
[2] Ken Evenson died on 29 January 2002.

0022-2852/$ - see front matter © 2003 Elsevier Inc. All rights reserved.
doi:10.1016/j.jms.2003.09.002

Table 1
Summary of the far-infrared LMR spectra of the ^{13}CH radical in the $v = 0$ level of the $X^2\Pi$ state

CO_2 pump	Gain medium	Wavelength (μm)	Frequency (MHz)	^{13}CH transitions observed		
				N	J	F_i[a]
9P(16)	CH_3OH	570.6	525 427.5	$1 \leftarrow 1$	$1\frac{1}{2} \leftarrow \frac{1}{2}$	$F_1 \leftarrow F_2$
10P(36)	CD_3I	556.9	538 347.3	$1 \leftarrow 1$	$1\frac{1}{2} \leftarrow \frac{1}{2}$	$F_1 \leftarrow F_2$
9R(6)	CH_2F_2	202.5	1 480 712.9	$2 \leftarrow 1$	$1\frac{1}{2} \leftarrow 1\frac{1}{2}$	$F_2 \leftarrow F_1$
10R(34)	CD_3OH	180.7	1 658 689.9	$2 \leftarrow 1$	$2\frac{1}{2} \leftarrow 1\frac{1}{2}$	$F_1 \leftarrow F_1$
10P(34)	CH_2DOH	124.4	2 409 293.3	$3 \leftarrow 2$	$2\frac{1}{2} \leftarrow 2\frac{1}{2}$	$F_2 \leftarrow F_1$
9P(36)	CH_3OH	118.8	2 522 781.6	$3 \leftarrow 2$	$3\frac{1}{2} \leftarrow 2\frac{1}{2}$	$F_1 \leftarrow F_1$

[a] F_i labels the spin components in order of increasing energy for a given J.

this reagent was both less convenient to handle and more expensive. The magnetic field was modulated at a frequency of 14 kHz and the signal detected with a lock-in amplifier at the same frequency. The resonances were consequently displayed as the first derivative of an absorption profile. The magnet of the LMR system was

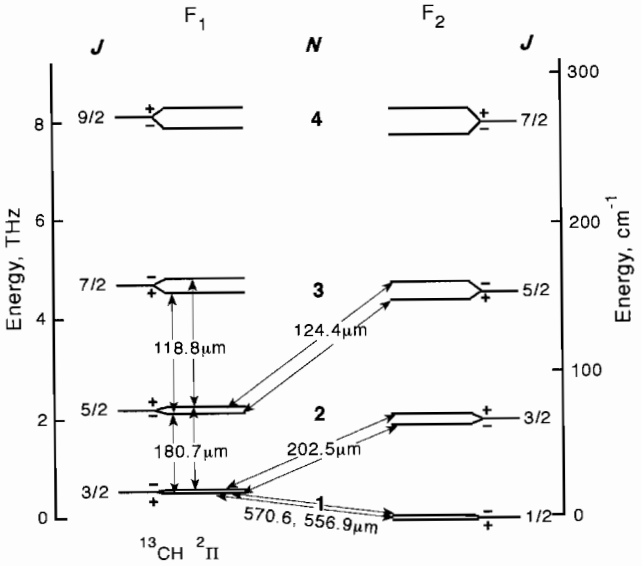

Fig. 1. Diagram showing the lower energy levels of the ^{13}CH radical in the $v = 0$ level of the $X^2\Pi$ state and the transitions involved in the observed far-infrared LMR spectrum. The lambda-type (parity) doubling has been exaggerated by a factor of 20 for the sake of clarity.

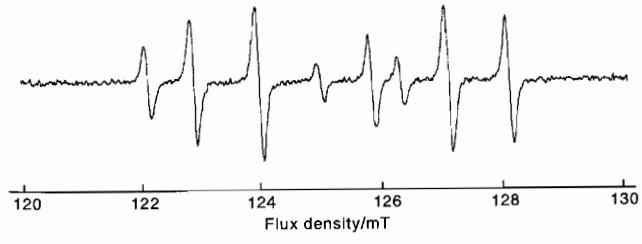

Fig. 2. Part of the far-infrared LMR spectrum of the ^{13}CH radical in the $v = 0$ level of the $X^2\Pi$ state. The spectrum is recorded with the 556.9 μm laser line in perpendicular polarization ($\Delta M_J = \pm 1$). The rotational transition involved is $N = 1 \leftarrow 1$, $J = 3/2 \leftarrow 1/2, - \leftarrow +$. The ^{13}C and ^1H hyperfine structure is fully resolved and many of the lines violate the nuclear spin selection rule $\Delta M_I = 0$ (see Table 2) because the spins remained coupled for the $J = 1/2$ level even in quite sizeable magnetic fields.

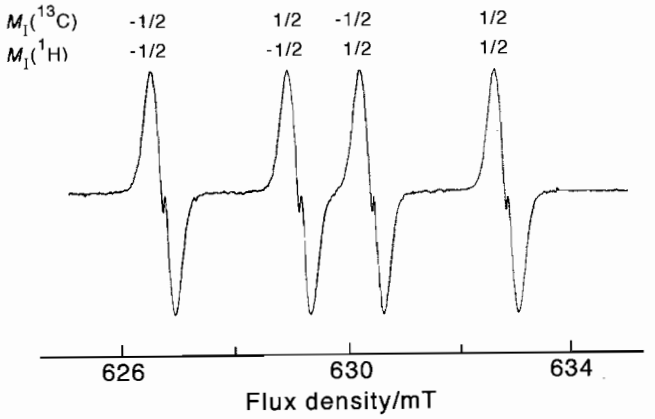

Fig. 3. Part of the far-infrared LMR spectrum of the ^{13}CH radical in the $v = 0$ level of the $X^2\Pi$ state, recorded with the 124.4 μm laser line in parallel polarization ($\Delta M_J = 0$). The transition involved is $N = 3 \leftarrow 2$, $J = 5/2 \leftarrow 5/2, - \leftarrow +$, $M_J = -5/2 \leftarrow -5/2$. Both the ^{13}C and ^1H hyperfine splittings are fully resolved at Doppler-limited resolution. The obvious Lamb dips at the centre of each resonance allow a more accurate measurement of the flux densities. The nuclear spin quantum numbers for the two central resonances are only approximate labels. The $M_F = 5/2$ levels are close to 50:50 mixtures of the $|M_{I_1} = 1/2, M_{I_2} = -1/2\rangle$ and $|M_{I_1} = -1/2, M_{I_2} = 1/2\rangle$ states.

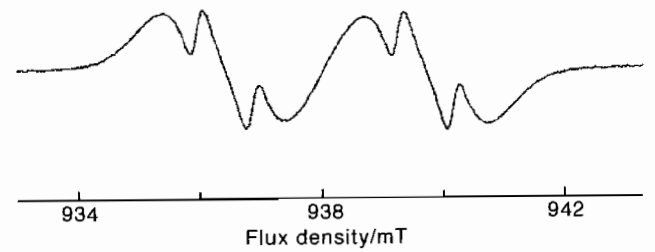

Fig. 4. A small part of the far-infrared LMR spectrum of the ^{13}CH radical in the $v = 0$ level of the $X^2\Pi$ state, recorded with the 118.8 μm laser line in parallel polarization ($\Delta M_J = 0$). The transition involved is $N = 3 \leftarrow 2$, $J = 7/2 \leftarrow 5/2, - \leftarrow +$, $M_J = -5/2 \leftarrow -5/2$. The ^{13}C hyperfine splitting is fully resolved at Doppler-limited resolution but the ^1H splittings are only observable as Lamb dips.

Table 2
Observations in the far-infrared LMR spectrum of the ^{13}CH radical in the $v = 0$ level of the $X^2\Pi$ state

$N' \leftarrow N''$	$J' \leftarrow J''$	Parity	$M_J' \leftarrow M_J''$	M_{I_1}[a]	M_{I_2}[a]	B_0 (mT)	$\nu_L - \nu_{calc}$ (MHz)	$\partial\nu/\partial B_0$ (MHz/mT)	Uncert. (MHz)
570.6 μm spectrum ν_L = 525427.5 MHz									
1 ← 1	3/2 ← 1/2	− ← +	−1/2 ← −1/2	1/2	−1/2	1939.91	−4.21	−4.93	10.0
					1/2	1941.28	−4.20	−4.93	10.0
				−1/2	−1/2	1947.10	−4.18	−4.92	10.0
					1/2	1948.49	−4.14	−4.92	10.0
		− ← +	−3/2 ← −1/2	1/2	−1/2	588.25	−0.73	−17.98	0.50
			−3/2 ← 1/2	−1/2	1/2 ← −1/2	588.94	0.85	−18.07	0.50
			−3/2 ← −1/2	1/2	1/2	589.45	−0.74	−17.98	0.50
			−3/2 ← −1/2	−1/2 ← 1/2	1/2	591.27	−1.23	−18.01	0.50
			−3/2 ← −1/2	−1/2	−1/2	591.99	−1.13	−17.97	0.50
				−1/2	1/2	593.22	−1.13	−17.97	0.50
		− ← +	−1/2 ← 1/2	1/2	−1/2	1914.36	5.76	−5.05	10.0
					1/2	1915.67	5.75	−5.05	10.0
				−1/2	−1/2	1916.60	5.04	−5.05	10.0
					1/2	1917.92	5.76	−5.11	10.0
556.9 μm spectrum ν_L = 538347.3 MHz									
1 ← 1	3/2 ← 1/2	− ← +	1/2 ← −1/2	1/2	−1/2 ← 1/2	362.82	−0.66	6.32	0.50
			1/2 ← −1/2	−1/2	−1/2 ← 1/2	364.39	−0.67	6.32	0.50
			1/2 ← 1/2	1/2	−1/2	367.84	0.85	6.22	0.50
			1/2 ← −1/2	−1/2 ← 1/2	1/2	368.50[b]	−0.81	6.28	0.86
			1/2 ← −1/2	−1/2 ← 1/2	−1/2	368.50[b]	−0.28	6.28	0.64
			1/2 ← 1/2	1/2 ← −1/2	−1/2 ← 1/2	369.79[b]	−1.60	6.26	0.94
			1/2 ← 1/2	1/2	1/2	369.79[b]	0.96	6.22	0.59
			1/2 ← 1/2	−1/2	−1/2	373.48	−0.08	6.23	0.52
			1/2 ← 1/2	−1/2 ← 1/2	1/2 ← −1/2	373.48	1.61	6.19	1.78
			1/2 ← 1/2	−1/2	1/2	375.21	0.41	6.22	0.50
		+ ← −	1/2 ← 1/2	−1/2	−1/2	949.68	−0.56	6.58	0.50
			1/2 ← −1/2	−1/2 ← 1/2	1/2	950.00	−0.43	6.57	0.50
			1/2 ← 1/2	1/2 ← −1/2	−1/2 ← 1/2	987.45	0.24	6.61	0.50
			1/2 ← −1/2	−1/2	−1/2 ← 1/2	993.74	−0.33	6.63	0.50
			1/2 ← 1/2	1/2	−1/2	994.99	0.22	6.60	0.50
			1/2 ← 1/2	1/2	1/2	997.74	0.40	6.59	0.50
			1/2 ← 1/2	−1/2	1/2	1000.11	0.12	6.60	0.50
			1/2 ← −1/2	−1/2 ← 1/2	−1/2	1003.95	−0.08	6.62	0.50
			1/2 ← 1/2	−1/2 ← 1/2	1/2 ← −1/2	1007.71	0.00	6.59	0.50
		− ← +	3/2 ← −1/2	1/2	−1/2 ← 1/2	122.09	0.64	18.20	0.50
			3/2 ← 1/2	1/2	−1/2	122.84	0.85	18.14	0.50
			3/2 ← 1/2	1/2 ← −1/2	−1/2 ← 1/2	123.93[b]	−0.63	18.12	1.04
			3/2 ← 1/2	1/2	1/2	123.93[b]	1.05	18.17	0.57
			3/2 ← −1/2	−1/2	−1/2 ← 1/2	124.94	0.70	18.22	0.50
			3/2 ← −1/2	−1/2 ← 1/2	−1/2	125.79	0.76	18.18	0.50
			3/2 ← −1/2	−1/2 ← 1/2	1/2	126.27	0.80	18.17	0.50
			3/2 ← 1/2	−1/2	−1/2	127.06	0.44	18.15	0.50
			3/2 ← 1/2	−1/2	1/2	128.05	0.50	18.14	0.50
		+ ← −	3/2 ← −1/2	−1/2 ← 1/2	1/2	332.43[b]	−0.53	18.26	0.75
			3/2 ← 1/2	−1/2	−1/2	332.43[b]	0.65	18.27	0.67
			3/2 ← 1/2	1/2	−1/2	340.41	0.17	18.29	0.50
			3/2 ← 1/2	1/2 ← −1/2	−1/2 ← 1/2	343.06	0.07	18.29	0.50
			3/2 ← 1/2	1/2	1/2	343.35	−0.16	18.27	0.50
			3/2 ← −1/2	−1/2	−1/2 ← 1/2	349.30	−0.24	18.29	0.50
			3/2 ← 1/2	−1/2 ← 1/2	1/2 ← −1/2	349.97	0.01	18.25	0.50
			3/2 ← −1/2	−1/2 ← 1/2	−1/2	352.30	−0.02	18.27	0.50
			3/2 ← 1/2	−1/2	1/2	352.61	0.09	18.25	0.70
		− ← +	1/2 ← −1/2	1/2	1/2	366.22[b]	−0.78	6.27	0.70
			1/2 ← −1/2	1/2	−1/2	366.22[b]	−0.25	6.27	0.50
			1/2 ← −1/2	−1/2	1/2 ← −1/2	367.76	−0.57	6.28	0.50
556.9 μm spectrum ν_L = 538347.3 MHz									
1 ← 1	3/2 ← 1/2	− ← +	1/2 ← −1/2	−1/2	−1/2	368.02	−0.64	6.29	0.50
			1/2 ← 1/2	1/2	1/2	371.15	0.23	6.22	0.50

Table 2 (*continued*)

$N' \leftarrow N''$	$J' \leftarrow J''$	Parity	$M_J' \leftarrow M_J''$	M_{I_1} [a]	M_{I_2} [a]	B_0 (mT)	$\nu_L - \nu_{calc}$ (MHz)	$\partial\nu/\partial B_0$ (MHz/mT)	Uncert. (MHz)
			1/2 ← 1/2	1/2 ← −1/2	1/2	372.94	0.32	6.21	0.50
		+ ← −	1/2 ← 1/2	1/2 ← −1/2	−1/2	943.40	0.05	6.56	0.50
			1/2 ← −1/2	1/2	1/2	943.73	0.05	6.56	0.50
			1/2 ← −1/2	1/2	−1/2	997.85	0.15	6.59	0.56
			1/2 ← −1/2	−1/2	1/2	1 000.27	−0.03	6.60	0.50
			1/2 ← 1/2	1/2	1/2 ← −1/2	1 001.55	0.53	6.58	0.50
			1/2 ← −1/2	−1/2	−1/2	1 006.54	−0.21	6.61	0.50
202.5 μm spectrum ν_L = 1 480 712.9 MHz									
2 ← 1	3/2 ← 3/2	+ ← −	−3/2 ← −3/2	−1/2	−1/2	629.55	−0.89	18.80	0.74
					1/2	632.03	−1.14	18.78	0.74
				1/2	−1/2	633.14	−1.06	18.80	0.74
					1/2	635.60	−1.59	18.78	0.74
		− ← +	−3/2 ← −3/2	1/2	−1/2	982.22	−0.69	18.35	0.74
					1/2	983.98	−0.89	18.36	0.74
				−1/2	−1/2	991.66	−0.64	18.35	0.74
					1/2	993.43	−1.14	18.35	0.74
		+ ← −	−1/2 ← −3/2	1/2	−1/2	669.30	−0.31	17.49	0.74
					1/2	670.87	−0.50	17.48	0.74
				−1/2	−1/2	671.22	0.02	17.51	0.74
					1/2	672.87	−0.21	17.51	0.74
		− ← +	−1/2 ← −3/2	1/2	−1/2	1 045.40	0.56	16.89	0.74
					1/2	1 045.72	0.43	16.90	0.74
				−1/2	−1/2	1 055.63	0.31	16.89	0.74
					1/2	1 055.94	0.15	16.89	0.74
180.7 μm spectrum ν_L = 1 658 689.9 MHz									
2 ← 1	5/2 ← 3/2	+ ← −	−3/2 ← −3/2	1/2	−1/2	890.15	−0.12	8.90	0.83
					1/2	890.35	−0.24	8.90	0.83
				−1/2	−1/2	894.59	0.43	8.90	0.83
					1/2	894.80	0.28	8.90	0.83
		− ← +	−3/2 ← −3/2	1/2	1/2	1 333.58	0.75	9.53	0.83
					−1/2	1 333.86	0.28	9.53	0.83
				−1/2	1/2	1 341.05	1.29	9.53	0.83
					−1/2	1 341.31	0.94	9.53	0.83
		+ ← −	−1/2 ← −1/2	1/2	−1/2	1 863.62	0.66	5.36	0.83
					1/2	1 864.27	0.44	5.36	0.83
				−1/2	−1/2	1 867.65	0.86	5.36	0.83
					1/2	1 868.32	0.51	5.36	0.83
		+ ← −	−1/2 ← −3/2	1/2	−1/2	487.31	0.04	15.58	0.83
					1/2	488.06	0.15	15.58	0.83
				−1/2	−1/2	490.70	0.27	15.57	0.83
					1/2	491.45	0.44	15.57	0.83
		+ ← −	1/2 ← −1/2	1/2	−1/2	733.90	−0.01	10.57	0.83
					1/2	735.00	−0.04	10.57	0.83
				−1/2	−1/2	736.73	0.09	10.57	0.83
					1/2	737.85	−0.08	10.56	0.83
		− ← +	−1/2 ← 1/2	1/2	−1/2	742.90[b]	1.41	16.05	1.17
					1/2	742.90[b]	1.59	16.05	1.17
				−1/2	−1/2	751.14[b]	1.03	16.05	1.17
					1/2	751.14[b]	1.15	16.05	1.17
		− ← +	1/2 ← −1/2	1/2	−1/2	1 107.81	1.14	11.07	0.83
					1/2	1 108.17	0.65	11.06	0.83
				−1/2	−1/2	1 115.53	0.52	11.07	0.83
					1/2	1 115.86	0.29	11.06	0.83
		+ ← −	3/2 ← 1/2	1/2	−1/2	1 487.66	−0.74	5.49	0.83
					1/2	1 488.97	−0.91	5.49	0.83
				−1/2	−1/2	1 489.70	−0.98	5.49	0.83
					1/2	1 490.98	−0.95	5.49	0.83
124.4 μm spectrum ν_L = 2 409 293.3 MHz									
3 ← 2	5/2 ← 5/2	− ← +	−5/2 ← −5/2	−1/2	−1/2	626.78	1.94	21.66	1.20
					1/2	629.14	1.38	21.65	1.20

Table 2 (*continued*)

$N' \leftarrow N''$ $J' \leftarrow J''$	Parity	$M_J' \leftarrow M_J''$	M_{I_1}[a]	M_{I_2}[a]	B_0 (mT)	$\nu_L - \nu_{calc}$ (MHz)	$\partial\nu/\partial B_0$ (MHz/mT)	Uncert. (MHz)
			1/2	−1/2	630.42	1.46	21.66	1.20
				1/2	632.78	1.12	21.65	1.20
	+ ← −	−5/2 ← −5/2	1/2	−1/2	1 088.31	0.98	20.70	1.20
				1/2	1 090.19	0.51	20.70	1.20
			−1/2	−1/2	1 097.50	0.62	20.70	1.20
				1/2	1 099.39	0.18	20.70	1.20
	− ← +	−3/2 ← −3/2	−1/2	−1/2	1 240.45	0.39	8.55	1.20
				1/2	1 245.03	0.80	8.56	1.20
			1/2	−1/2	1 245.09	−0.55	8.54	1.20
				1/2	1 249.68	−0.23	8.55	1.20
	− ← +	3/2 ← −5/2	−1/2	−1/2	708.61	1.51	18.73	1.20
				1/2	709.58	1.46	18.72	1.20
			1/2	−1/2	711.55	1.24	18.74	1.20
				1/2	712.53	1.02	18.73	1.20
	− ← +	−5/2 ← −3/2	−1/2	−1/2	968.98	0.60	12.76	1.20
				1/2	974.05	0.36	12.75	1.20
			1/2	−1/2	974.45	0.02	12.76	1.20
				1/2	979.52	−0.21	12.76	1.20
	+ ← −	−3/2 ← −5/2	1/2	−1/2	1 247.58	2.09	17.23	1.20
				1/2	1 248.83	1.65	17.23	1.20
			−1/2	−1/2	1 258.00	1.20	17.22	1.20
				1/2	1 259.24	0.88	17.23	1.20
	− ← +	−1/2 ← −3/2	−1/2	−1/2	1 799.46	0.30	4.02	1.20
				1/2	1 802.77[b]	0.02	3.85	1.70
			1/2	−1/2	1 802.77[b]	0.44	3.87	1.70
				1/2	1 806.07	0.17	3.86	1.20
	+ ← −	−5/2 ← −3/2	1/2	−1/2	1 849.27	−1.99	9.36	1.20
				1/2	1 851.93	−2.00	9.37	1.20
			−1/2	−1/2	1 863.53	−1.79	9.36	1.20
				1/2	1 866.19	−1.87	9.37	1.20
118.8 μm spectrum $\nu_L = 2\,522\,781.6$ MHz								
3 ← 2 7/2 ← 5/2	− ← +	−5/2 ← −5/2	1/2	−1/2	936.11	0.13	7.08	1.26
				1/2	937.03	0.07	7.07	1.26
			−1/2	−1/2	939.44	0.36	7.07	1.26
				1/2	940.35	0.36	7.07	1.26
	− ← +	−3/2 ← −3/2	1/2	−1/2	1 369.83	−0.21	5.31	1.26
				1/2	1 370.84	−0.35	5.31	1.26
			−1/2	−1/2	1 373.12	−0.06	5.31	1.26
				1/2	1 374.12	−0.09	5.31	1.26
	+ ← −	−5/2 ← −5/2	1/2	−1/2	1 737.67	−0.57	8.96	1.26
				1/2	1 738.43	−0.40	8.96	1.26
			−1/2	−1/2	1 742.74	0.90	8.95	1.26
				1/2	1 743.51	0.97	8.95	1.26
	− ← +	−3/2 ← −5/2	1/2	−1/2	530.73	0.70	11.60	1.26
				1/2	532.04	0.47	11.60	1.26
			−1/2	−1/2	533.27	0.74	11.59	1.26
				1/2	534.56	0.44	11.59	1.26
	− ← +	−1/2 ← −3/2	1/2	−1/2	669.03	0.29	8.61	1.26
				1/2	670.42	0.42	9.19	1.26
			−1/2	−1/2	671.37	0.33	9.19	1.26
				1/2	672.76	0.44	9.10	1.26
	− ← +	1/2 ← −1/2	1/2	−1/2	906.72	0.51	6.78	1.26
				1/2	908.31	0.47	6.78	1.26
			−1/2	−1/2	908.73	0.40	6.78	1.26
				1/2	910.32	0.38	6.78	1.26
	+ ← −	−3/2 ← −5/2	1/2	−1/2	1 045.38	−1.19	13.05	1.26
				1/2	1 046.04	−1.14	13.04	1.26
			−1/2	−1/2	1 051.95	−1.49	13.05	1.26
				1/2	1 052.61	−1.44	13.05	1.26
	+ ← −	−1/2 ← −3/2	1/2	−1/2	1 319.69	−1.47	10.17	1.26
				1/2	1 320.40	−1.54	10.22	1.26
			−1/2	−1/2	1 326.26	−1.68	10.23	1.26

Table 2 (*continued*)

$N' \leftarrow N''$ $J' \leftarrow J''$	Parity	$M'_J \leftarrow M''_J$	M_{I_1}[a]	M_{I_2}[a]	B_0 (mT)	$\nu_L - \nu_{calc}$ (MHz)	$\partial\nu/\partial B_0$ (MHz/mT)	Uncert. (MHz)
				1/2	1 326.98	−1.80	10.23	1.26
	− ← +	3/2 ← 1/2	1/2	−1/2	1 418.71	−0.60	4.27	1.26
			−1/2	−1/2	1 420.31	−2.19	4.26	1.26
			−1/2	−1/2	1 420.73	−0.70	4.27	1.26
			−1/2	1/2	1 422.00	−0.89	4.26	1.26
	+ ← −	1/2 ← −1/2	−1/2	−1/2	1 802.64	−1.31	7.26	1.26
				1/2	1 803.41	−1.36	7.26	1.26
			−1/2	−1/2	1 809.24	−1.18	7.26	1.26
				1/2	1 809.98	−0.98	7.26	1.26

[a] I_1 and I_2 are the nuclear spins of the ^{13}C and ^{1}H nuclei, respectively. Transitions obey the allowed nuclear spin selection rule $\Delta M_{I_1} = \Delta M_{I_2} = 0$ unless indicated.

[b] Resonances not resolved.

controlled by a rotating-coil magnetometer which provided a direct readout of the flux densities. The system was calibrated periodically up to 1.8 T with a proton NMR gaussmeter; the absolute uncertainty was 10^{-5} T below 0.1 T and the fractional uncertainty was 10^{-4} above 0.1 T.

3. Results and analysis

3.1. Observations and assignments

The far-infrared observations on ^{13}CH in the $v = 0$ level are summarised in Table 1 and are shown on the energy level diagram in Fig. 1. Resonances associated with five separate rotational transitions have been observed all together. An example from the 556.9 μm spectrum is shown in Fig. 2. The transition involved is $N = 1 \leftarrow 1$, $J = 3/2 \leftarrow 1/2$. Both the ^{13}C and ^{1}H nuclear hyperfine structures (both nuclei have $I = 1/2$) are clearly resolved; many of the signals are nuclear spin-forbidden transitions which occur with significant intensity for transitions which involve the unique $J = 1/2$ level. Most of the resonances recorded were observed with sub-Doppler accuracy as Lamb dips. An example of the signals obtained when both the ^{13}C and ^{1}H nuclear hyperfine splittings are already fully resolved at Doppler-limited resolution is shown in Fig. 3. The spectrum involved in this case is associated with the $N = 3 \leftarrow 2$, $J = 5/2 \leftarrow 5/2$ transition and was recorded with the 124.4 μm laser line. Another rather beautiful example of Lamb dips is shown in Fig. 4. In this case, from the 118.8 μm spectrum, the proton hyperfine is not resolved at Doppler resolution but is through the observation of the Lamb dips.

The detailed measurements for the six laser lines used to record LMR spectra are given in Table 2. The assignments were made with the help of a computer program which predicts all possible resonances for a given laser frequency, together with their linestrengths and tuning rates [3,21]. This information constitutes the Zeeman pattern which can be used to make the assignments even when the molecular parameters employed are not quite accurate. The molecular parameters were estimated from the corresponding values for CH [3,4] using appropriate isotopic scaling factors. The resultant assignments are also given in Table 2. The quantum numbers used to describe the molecular states are N, J, parity, M_J, M_{I_1} and M_{I_2} where I_1 and I_2 refer to the ^{13}C and ^{1}H nuclei, respectively. The nuclear spin de-coupled description is the appropriate one for experiments performed in a magnetic field although several somewhat weaker transitions which violate the selection rule $\Delta M_I = 0$ were observed, see Table 2. An estimate of the experimental uncertainty of each observation is given in the Table; this is dominated by the accuracy of the far-infrared laser frequencies which are re-settable to $\sqrt{2} \times 5 \times 10^{-7} \nu_L$.

3.2. Determination of molecular parameters

A nearly complete set of molecular parameters for ^{13}CH in the $v = 0$ level of its $X^2\Pi$ state was determined by fitting a model Hamiltonian to the present measurements combined with those of the lambda-doubling spectrum [17] by least-squares methods. The effective Hamiltonian was cast in the N^2 form as described by Brown et al. [22] with the Zeeman terms as described in [23]. This is the same Hamiltonian as was used in the earlier work on the far-infrared LMR spectrum of CH [3] and CD [10]. The eigenstates were identified in terms of Hund's case (b) quantum numbers as described above. The basis set was truncated at states with $\Delta N = \pm 2$ which reproduced the exact calculations to within a few kHz for the highest field resonances. Each datum was weighted in the fit inversely as the square of its experimental error, whose values are given in Table 2. The parameter A_D was constrained to zero in the fit as a result of which the parameters A and γ are effective parameters [24].

Table 3
Fit of the lambda-doubling transition frequencies of the ^{13}CH radical in the $v = 0$ level of the $X^2\Pi$ state

$N' \leftarrow N''$	$J' \leftarrow J''$	Parity	$F_1' \leftarrow F_1''$[a]	$F' \leftarrow F''$	ν (MHz)	$\nu_{obs} - \nu_{calc}$ (MHz)	Uncert. (MHz)
2	5/2	$+ \leftarrow -$	$3 \leftarrow 3$	$7/2 \leftarrow 7/2$	4712.13	−0.39	0.45
				$5/2 \leftarrow 5/2$	4734.34	−0.31	0.60
				$5/2 \leftarrow 7/2$	4743.92	0.32	2.20
			$2 \leftarrow 2$	$5/2 \leftarrow 3/2$	4848.36	2.77	2.50
				$5/2 \leftarrow 5/2$	4855.63	1.10	0.45
				$3/2 \leftarrow 3/2$	4878.25	1.58	0.60
				$3/2 \leftarrow 5/2$	4887.73	2.12	2.00
				$7/2 \leftarrow 5/2$	4899.75	4.32	1.80
3	7/2	$- \leftarrow +$	$4 \leftarrow 4$	$9/2 \leftarrow 9/2$	11047.51	−2.07	0.70
				$7/2 \leftarrow 7/2$	11070.85	−0.82	1.00
			$3 \leftarrow 3$	$7/2 \leftarrow 7/2$	11190.16	0.51	0.02
				$5/2 \leftarrow 5/2$	11212.77	1.02	0.54
1	1/2	$- \leftarrow +$	$0 \leftarrow 1$	$1/2 \leftarrow 3/2$	3030.26	1.00	1.00
				$1/2 \leftarrow 1/2$	3041.14	0.49	1.25
			$1 \leftarrow 0$	$1/2 \leftarrow 1/2$	3323.30	0.43	0.75
			$1 \leftarrow 1$	$1/2 \leftarrow 3/2$	3343.94	0.14	1.30
				$1/2 \leftarrow 1/2$	3355.73	0.54	1.00
			$1 \leftarrow 0$	$3/2 \leftarrow 1/2$	3373.57	0.01	0.75
			$1 \leftarrow 1$	$3/2 \leftarrow 3/2$	3394.58	0.09	0.65
				$3/2 \leftarrow 1/2$	3406.53	0.66	2.00
2	3/2	$+ \leftarrow -$	$1 \leftarrow 1$	$1/2 \leftarrow 3/2$	7093.95	1.69	2.20
				$1/2 \leftarrow 1/2$	7144.53	2.52	1.50
				$3/2 \leftarrow 3/2$	7159.27	2.19	1.35
				$3/2 \leftarrow 1/2$	7210.11	3.27	1.20
			$2 \leftarrow 1$	$3/2 \leftarrow 3/2$	7245.41	0.58	1.25
			$2 \leftarrow 2$	$3/2 \leftarrow 3/2$	7296.91	−0.21	1.30
				$5/2 \leftarrow 5/2$	7309.94	−2.25	1.25
				$5/2 \leftarrow 3/2$	7363.69	1.74	2.00
3	5/2	$- \leftarrow +$	$2 \leftarrow 2$	$3/2 \leftarrow 5/2$	14458.28	1.79	2.50
				$3/2 \leftarrow 3/2$	14499.52	0.85	0.80
				$5/2 \leftarrow 5/2$	14515.81	−1.26	0.70
			$2 \leftarrow 3$	$3/2 \leftarrow 5/2$	14539.69	0.25	2.50
			$3 \leftarrow 2$	$5/2 \leftarrow 5/2$	14561.96	0.61	2.00
			$2 \leftarrow 3$	$5/2 \leftarrow 5/2$	14599.89	−0.13	2.20
			$3 \leftarrow 2$	$7/2 \leftarrow 5/2$	14623.54	1.61	2.20
			$3 \leftarrow 3$	$5/2 \leftarrow 5/2$	14643.93	−0.37	0.50
				$7/2 \leftarrow 7/2$	14662.00	−0.70	0.50
				$7/2 \leftarrow 5/2$	14704.94	0.06	2.50

[a] Coupling scheme: $\boldsymbol{J} = \boldsymbol{N} + \boldsymbol{S}$; $\boldsymbol{F_1} = \boldsymbol{J} + \boldsymbol{I_1}$; $\boldsymbol{F} = \boldsymbol{F_1} + \boldsymbol{I_2}$; where I_1 and I_2 are the ^{13}C and ^{1}H nuclear spins, respectively.

The results of the least-squares fit are given in Tables 2 and 3; the parameters determined in the process are given in Table 4 in both MHz and cm^{-1} units. Some of the smaller parameters (H, γ_D, p_H and q_H) have been constrained to values estimated from other sources [23,25]. The values adopted are given in the Table. The electron spin g-factor was fixed to a value of 2.0020, which corresponds to a relativistic correction of 1.5×10^{-4}. The values for the four proton hyperfine parameters were constrained to the values determined from the more accurate measurements for ^{12}CH [6]. The standard deviation of the fit of 221 data points relative to experimental uncertainties is 1.038, a figure which can be regarded as entirely satisfactory (a value of 1.0 is expected if the model is adequate and the weighting factors have been chosen correctly).

4. Discussion

The measurements from the far-infrared LMR spectrum of ^{13}CH in the $v = 0$ level of its $X^2\Pi$ state have allowed the determination of a complete set of molecular parameters in the effective Hamiltonian, including the ^{13}C hyperfine parameters. The values obtained for the major parameters are in reasonably good agreement with those obtained by Zachwieja from optical spectroscopy [13] as can be seen from the comparison in Table 5. However the values determined in the present work are considerably more accurate; we have also been able to obtain a value for the spin-orbit coupling constant A_0 whereas Zachwieja had to use a value scaled from that for ^{12}CH. Zachwieja also determined the parameters which describe the vibrational dependence of

Table 4
Molecular parameters for ^{13}CH in the $v = 0$ level of the $X^2\Pi$ state

Parameter	Value (MHz)	Value (cm^{-1})
$\tilde{A}$	843 799.44 (41)[a]	28.146120 (14)
$\tilde{\gamma}$	−765.10 (12)	−0.0255209 (40)
$\tilde{\gamma}_D$	0.156[b]	0.520×10^{-5}[b]
B	422 966.021 (95)	14.1086278 (32)
D	43.3291 (48)	$0.144530\ (16) \times 10^{-2}$
H	0.308×10^{-2}[b]	0.1027×10^{-6}[b]
p	998.39 (24)	0.0333026 (80)
p_D	−0.305 (23)	$-0.1016\ (76) \times 10^{-4}$
p_H	0.334×10^{-4}[b]	0.1114×10^{-8}[b]
q	1 146.073 (44)	$0.382289\ (15) \times 10^{-1}$
q_D	−0.4554 (39)	$-0.1519\ (13) \times 10^{-4}$
q_H	$0.941\ 2 \times 10^{-4}$[b]	$0.314\ 0 \times 10^{-8}$[b]
a (^{13}C)	218.10 (42)	$0.7275\ (14) \times 10^{-2}$
b_F (^{13}C)	41.99 (28)	$0.14007\ (93) \times 10^{-2}$
c (^{13}C)	−131.0 (12)	$-0.4369\ (39) \times 10^{-2}$
d (^{13}C)	275.54 (26)	$0.91911\ (86) \times 10^{-2}$
a (^{1}H)	54.006[b]	0.18014×10^{-2}[b]
b_F (^{1}H)	−57.777[b]	-0.1927×10^{-2}[b]
c (^{1}H)	56.52[b]	0.3455×10^{-2}[b]
d (^{1}H)	43.513[b]	0.14514×10^{-2}[b]
g'_L	1.000937 (42)	
g_S	2.0020[b]	
g_l	$0.1806\ (52) \times 10^{-2}$	
g_r	$-0.285\ 4(11) \times 10^{-2}$	
g'_l	$0.1488(34) \times 10^{-2}$	
g^{ef}_r	$-0.2606\ (17) \times 10^{-2}$	
g_N (^{13}C)	1.404824[c]	
g_N (^{1}H)	5.585695[c]	

[a] Numbers in parentheses are one standard deviation of the least-squares fit, in units of the last quoted decimal place.
[b] Parameter constrained to this value in the fit (see text).
[c] Nuclear spin g-factors in nuclear magnetons.

the rotational constant. These can be combined with our value for B_0 to determine the value at the equilibrium bond length, $B_e = 14.37366(12)\,cm^{-1}$. This corresponds to a value for r_e of 1.119777(5) Å, slightly different from the corresponding value for ^{12}CH (1.119788(5) Å [26]). The difference arises from the non-adiabatic corrections to the value for B_e [27]. These have to be taken into account if the correct Born–Oppenheimer value for the equilibrium bond length is to be obtained.

The values for the lambda-type doubling and nuclear hyperfine parameters for ^{13}CH determined here (Table 4) differ somewhat from those determined previously [17]. In fact the present work represents a significant improvement in our knowledge of the lambda-doubling intervals; the hyperfine splittings in particular are determined more accurately because most of the signals in the LMR spectra were recorded as Lamb dips. This result points up the rather large uncertainties in the lambda-doubling frequencies as measured by microwave-optical double resonance [17], see Table 3. There is a need to measure them more accurately by direct absorption methods. The interpretation of the ^{13}C hyperfine parameters has been discussed in some detail by earlier authors [17,19]. The remarks made in those papers apply equally well to the present results.

The values for the molecular parameters for ^{12}CH are now known very accurately [5,6]. The values for corresponding parameters for ^{13}CH are related to these by comparatively simple isotopic scaling factors [22,25]. The predicted values for the major parameters for ^{13}CH obtained using these scaling factors are also given in Table 5. It can be seen that, although the values compare well with the experimentally determined parameters, the differences are much greater than the estimated uncertainties. This is a well-known manifestation of the breakdown of the Born–Oppenheimer separation [28].

As can be seen in Table 4, we have been able to determine five of the six possible g-factors for a molecule in a $^2\Pi$ state. The orbital g-factor g'_L deviates from unity because of relativistic and non-adiabatic corrections [29]. The former is typically about -1.5×10^{-4}, from which the non-adiabatic correction, Δg_L is calculated to be $1.087(42) \times 10^{-3}$. The rotational g-factor g_r has nuclear and electronic contributions:

$$g_r = g_r^N - g_r^e. \tag{1}$$

The nuclear contribution depends only on the nuclear masses and charges for a diatomic molecule; for ^{13}CH, it is calculated to be 0.5234×10^{-3} (in units of Bohr magnetons) leaving g_r^e as $0.3377(11) \times 10^{-2}$. The two

Table 5
Comparison of molecular parameters for ^{13}CH in the $v = 0$ level of the $X^2\Pi$ state

Parameter[a]	Present work	Previous work[b]	Scaled from ^{12}CH[c]
B_0	14.1086278 (32)	14.108141 (57)	14.108278
D_0	$0.144530\ (16) \times 10^{-2}$	$0.144410\ (16) \times 10^{-2}$	0.144352×10^{-2}
$\tilde{A}_0$	28.146120 (14)	28.14643[d]	28.146537
$\tilde{\gamma}_0$	$-0.255209\ (40) \times 10^{-1}$	$-0.2551\ (28) \times 10^{-1}$	-0.25304×10^{-1}
p_0	$0.333026\ (80) \times 10^{-1}$	$0.3313\ (15) \times 10^{-1}$	0.332961×10^{-1}
q_0	$0.382289\ (15) \times 10^{-1}$	$0.3819\ (12) \times 10^{-1}$	0.382238×10^{-1}

[a] Values given in cm^{-1}.
[b] Values determined by Zachwieja [13].
[c] Value calculated by isotopic scaling of the corresponding value for ^{12}CH in its $X^2\Pi$ state [3,4,26]. The ratio of the reduced masses $\mu(^{13}CH)/\mu(^{12}CH)$ is 1.006014282.
[d] Parameter constrained to this value, obtained by isotopic scaling from ^{12}CH, in the fit [13].

Table 6
Calculated spin-rotation transition frequencies of the ^{13}CH radical in the $v = 0$ level of the $X^2\Pi$ state

$N' \leftarrow N''$	$J' \leftarrow J''$	Parity	$F_1' \leftarrow F_1''$[a]	ν(MHz)	Vacuum wavelength(μm)	Line strength[b] $S_{F'F}$
$2 \leftarrow 1$	$5/2 \leftarrow 3/2$	$- \leftarrow +$	$2 \leftarrow 1$	1 647 239.4(20)[c]	181.99690	1.4839
			$2 \leftarrow 2$	1 647 016.2(20)	182.02156	0.1648
			$3 \leftarrow 2$	1 647 239.4(20)	182.00132	2.3083
		$+ \leftarrow -$	$2 \leftarrow 1$	1 652 326.3(20)	181.54647	1.4850
			$2 \leftarrow 2$	1 651 250.0(20)	181.55486	0.1651
			$3 \leftarrow 2$	1 651 291.4(20)	181.55031	2.3103
$3 \leftarrow 2$	$7/2 \leftarrow 5/2$	$- \leftarrow +$	$3 \leftarrow 2$	2 517 015.2(20)	119.10633	2.6139
			$3 \leftarrow 3$	2 516 973.8(20)	119.10829	0.1308
			$4 \leftarrow 3$	2 516 998.3(20)	119.10714	3.5290
		$+ \leftarrow -$	$3 \leftarrow 2$	2 510 679.5(20)	119.40690	2.6131
			$3 \leftarrow 3$	2 510 496.4(20)	119.41561	0.1306
			$4 \leftarrow 3$	2 510 660.9(20)	119.40779	3.5277
$4 \leftarrow 3$[d]	$9/2 \leftarrow 7/2$	$- \leftarrow +$	$4 \leftarrow 3$	3 356 953.5(40)	89.30492	3.6916
			$4 \leftarrow 4$	3 356 789.0(40)	89.30930	0.1054
			$5 \leftarrow 4$	3 356 942.6(40)	89.30521	4.6408
		$+ \leftarrow -$	$4 \leftarrow 3$	3 365 515.1(40)	89.07773	3.6922
			$4 \leftarrow 4$	3 365 490.6(40)	89.07838	0.1056
			$5 \leftarrow 4$	3 365 505.0(40)	89.07800	4.6418
$2 \leftarrow 1$[d]	$3/2 \leftarrow 1/2$	$- \leftarrow +$	$1 \leftarrow 0$	1 997 423.2(40)	150.08960	0.3331
			$1 \leftarrow 1$	1 997 446.4(40)	150.08786	0.1666
			$2 \leftarrow 1$	1 997 443.7(40)	150.08806	0.8327
		$+ \leftarrow -$	$1 \leftarrow 0$	2 001 567.2(40)	149.77886	0.3345
			$1 \leftarrow 1$	2 001 223.0(40)	149.80463	0.1673
			$2 \leftarrow 1$	2 001 367.3(40)	149.79383	0.8365
$3 \leftarrow 2$[d]	$5/2 \leftarrow 3/2$	$- \leftarrow +$	$2 \leftarrow 1$	2 578 047.8(40)	116.28662	1.4858
			$2 \leftarrow 2$	2 577 903.5(40)	116.29313	0.1651
			$3 \leftarrow 2$	2 578 003.8(40)	116.28860	2.3113
		$+ \leftarrow -$	$2 \leftarrow 1$	2 570 692.6(40)	116.61933	1.4845
			$2 \leftarrow 2$	2 570 695.3(40)	116.61921	0.1650
			$3 \leftarrow 2$	2 570 653.9(40)	116.62109	2.3092
$4 \leftarrow 3$[d]	$7/2 \leftarrow 5/2$	$- \leftarrow +$	$3 \leftarrow 2$	3 387 172.7(40)	88.50817	2.6132
			$3 \leftarrow 3$	3 387 214.1(40)	88.50709	0.1307
			$4 \leftarrow 3$	3 387 154.7(40)	88.50864	3.5278
		$+ \leftarrow -$	$3 \leftarrow 2$	3 396 728.3(40)	88.25918	2.6141
			$3 \leftarrow 3$	3 396 628.0(40)	88.26179	0.1306
			$4 \leftarrow 3$	3 396 708.5(40)	88.25970	3.5292
$1 \leftarrow 1$	$3/2 \leftarrow 1/2$	$- \leftarrow +$	$1 \leftarrow 0$	536 014.3(20)	559.29939	0.3353
			$1 \leftarrow 1$	536 037.5(20)	559.27516	0.1666
			$2 \leftarrow 1$	536 113.8(20)	559.19560	0.8341
		$+ \leftarrow -$	$1 \leftarrow 0$	532 225.0(20)	563.28142	0.3320
			$1 \leftarrow 1$	531 880.8(20)	563.64594	0.1662
			$2 \leftarrow 1$	532 104.0(20)	563.40952	0.8302
$2 \leftarrow 1$	$3/2 \leftarrow 3/2$	$- \leftarrow +$	$1 \leftarrow 1$	1 462 185.7(20)	205.03036	0.1680
			$1 \leftarrow 2$	1 461 962.5(20)	205.06167	0.0336
			$2 \leftarrow 1$	1 462 183.0(20)	205.03074	0.0336
			$2 \leftarrow 2$	1 461 959.8(20)	205.06204	0.3028
		$+ \leftarrow -$	$1 \leftarrow 1$	1 468 565.5(20)	204.13966	0.1652
			$1 \leftarrow 2$	1 468 489.2(20)	204.15026	0.0330
			$2 \leftarrow 1$	1 468 709.7(20)	204.11961	0.0331
			$2 \leftarrow 2$	1 468 633.5(20)	204.13021	0.2972
$3 \leftarrow 2$	$5/2 \leftarrow 5/2$	$- \leftarrow +$	$2 \leftarrow 2$	2 395 287.0(20)	125.15930	0.1323
			$2 \leftarrow 3$	2 395 245.6(20)	125.16147	0.0094
			$3 \leftarrow 2$	2 395 387.3(20)	125.15407	0.0095
			$3 \leftarrow 3$	2 395 345.9(20)	125.15623	0.1888
		$+ \leftarrow -$	$2 \leftarrow 2$	2 385 638.9(20)	125.66548	0.1344
			$2 \leftarrow 3$	2 385 455.7(20)	125.67513	0.0096
			$3 \leftarrow 2$	2 385 597.5(20)	125.66766	0.0096
			$3 \leftarrow 3$	2 385 414.4(20)	125.67731	0.1921
$4 \leftarrow 3$[d]	$7/2 \leftarrow 7/2$	$- \leftarrow +$	$3 \leftarrow 3$	3 262 132.1(40)	91.90077	0.1079
			$3 \leftarrow 4$	3 261 967.6(40)	91.90541	0.0040
			$4 \leftarrow 3$	3 262 072.7(40)	91.90245	0.0040
			$4 \leftarrow 4$	3 261 908.2(40)	91.90708	0.1401

Table 6 (*continued*)

$N' \leftarrow N''$	$J' \leftarrow J''$	Parity	$F_1' \leftarrow F_1''$[a]	ν(MHz)	Vacuum wavelength(μm)	Line strength[b] $S_{F'F}$
		$+ \leftarrow -$	$3 \leftarrow 3$	3 275 000.1(40)	91.53968	0.1064
			$3 \leftarrow 4$	3 274 975.7(40)	91.54036	0.0039
			$4 \leftarrow 3$	3 275 080.6(40)	91.53743	0.0040
			$4 \leftarrow 4$	3 275 056.1(40)	91.53811	0.1377

[a] Coupling scheme: $\boldsymbol{J} = \boldsymbol{N} + \boldsymbol{S}$; $\boldsymbol{F_1} = \boldsymbol{J} + \boldsymbol{I_1}$; $\boldsymbol{F} = \boldsymbol{F_1} + \boldsymbol{I_2}$ where $\boldsymbol{I_1}$ and $\boldsymbol{I_2}$ are the ^{13}C and ^{1}H nuclear spins, respectively. The proton hyperfine splittings are not included.

[b] For definition, see Eq. (4).

[c] Estimated uncertainty in units of the last quoted decimal place (1σ).

[d] Transition not directly studied in the LMR experiment.

parameters Δg_L and g_r^e have essentially the same physical origin in the effective Hamiltonian, both depending on the admixture of $^2\Sigma$ and $^2\Delta$ states [29]. However, while Δg_L depends on the difference of these two effects, g_r^e depends on their sum. Thus if a $^2\Pi$ state is contaminated by $^2\Sigma$ states alone, Δg_L is equal to g_r^e. Our experimental result shows that this is clearly not the case and we thus have evidence that both $^2\Sigma$ and $^2\Delta$ states are mixed into the $X^2\Pi$ state of CH. The next g-factor determined in our fit is g_l, the anisotropic correction to the electron spin magnetic moment. The value in Table 4 ($0.1806(52) \times 10^{-2}$) does not agree well with the expectations of Curl's relationship [30], $-\gamma/2B$ or 0.904×10^{-2}. This is because γ is an effective parameter in our fit, containing a contribution from the parameter A_D also [24]. Finally, estimates for the two lambda-doubling g-factors can be made from the relationships

$$g_l' = p/2B, \tag{2}$$

$$g_r^{e'} = -q/B, \tag{3}$$

which proved very reliable for OH [23]. The values obtained from these equations are 0.1355×10^{-2} and -0.2711×10^{-2}, in good agreement with the values determined in Table 4.

CH was one of the first molecules to be identified in the interstellar medium (ISM) through the detection of a single line in the $A^2\Delta$–$X^2\Pi$ electronic transition [31,32]. Its presence in the ISM was dramatically confirmed in 1973 by radio astronomy through the detection of lambda-doubling transitions in the lowest rotational level ($J = 1/2$) around 3.3 GHz [2]. More recently, ^{12}CH has also been detected in the ISM by the observation of the $J = 3/2 - 1/2$, $F_2 - F_2$ transition at 149 μm using instruments on the Kuiper Airborne Observatory [33] and on the ISO satellite [34]. Since a measurement of the relative abundance of different isotopes provides valuable information on star formation processes, it is desirable to measure the corresponding transitions in ^{13}CH as well. We have therefore used the parameters in Table 4 to calculate the zero-field rotational spectrum of ^{13}CH. The computed values of the transition frequencies for levels up to $N = 4$ are given in Table 6. For the sake of simplicity, the relatively small proton hyperfine splittings have not been included. The computed linestrengths $S_{F'F}$, which are also listed in Table 6, can be used to assess the relative intensities of individual transitions. The linestrength is defined by

$$S_{F'F} = |\langle \gamma' F' \| D_{.q}^{(1)}(\omega)^* \| \gamma F \rangle|^2, \tag{4}$$

where the quantity on the right-hand side is the reduced matrix element of the rotation matrix [35] and γ stands for subsidiary quantum numbers. The intensity of the line in absorption can be obtained by multiplying the linestrength by the square of the dipole moment μ (1.40 Debye for CH [36,37]), by the transition frequency and by the population difference between the lower and upper states. The Einstein A-coefficients for spontaneous emission from state i to j can also be calculated from the linestrengths by use of the relation

$$A_{i\to j} = (16\pi^3 \nu_{ij}^3 / 3\varepsilon_0 hc^3)(2F_i + 1)^{-1} S_{ij}\mu^2. \tag{5}$$

Table 6 is not quite complete because the transitions with $\Delta J = 1$, $F_2 \leftarrow F_1$ have been omitted. Although these transitions are formally allowed, they are very weak because they also require $\Delta N = 2$ and so would be forbidden in the Hund's case (b) limit (to which CH conforms closely in its ground $^2\Pi$ state).

Acknowledgments

We are grateful to Dr. Jonathan Towle for development of the computer program used in this work and to Dr. Tom Varberg for a critical reading of the manuscript. The study was supported in part by NASA contract W15,047.

References

[1] K.-P. Huber, G. Herzberg, Constants of Diatomic Molecules, Van Nostrand Reinhold, New York, 1979.

[2] O.E.H. Rydbeck, J. Elldér, W.M. Irvine, Nature 246 (1973) 466–468.

[3] J.M. Brown, K.M. Evenson, J. Mol. Spectrosc. 98 (1983) 392–403.
[4] C.R. Brazier, J.M. Brown, Can. J. Phys. 62 (1984) 1563–1578.
[5] T. Amano, Astrophys. J. Lett. 531 (2000) L161–L164.
[6] S.A. Davidson, K.M. Evenson, J.M. Brown, Astrophys. J. 546 (2000) 330–337.
[7] G. Herzberg, J.W.C. Johns, Astrophys. J. 158 (1969) 399–418.
[8] I. Morino, K. Matsumura, K. Kawaguchi, J. Mol. Spectrosc. 174 (1995) 123–131.
[9] M. Wienkoop, W. Urban, J.P. Towle, J.M. Brown, K.M. Evenson, J. Mol. Spectrosc. 208 (2003) 85–94.
[10] J.M. Brown, K.M. Evenson, J. Mol. Spectrosc. 136 (1989) 68–85.
[11] J. Richter, K.-F. Tonner, Astrophys. J. 67 (1967) 155–164.
[12] S.M. Anderson, K.E. McMurdy, Chem. Phys. Lett. 157 (1989) 531–534.
[13] M. Zachwieja, J. Mol. Spectrosc. 182 (1997) 18–33.
[14] A. Para, J. Phys. B 24 (1991) 3179–3185.
[15] Z. Bembenek, R. Kepa, M. Rytel, J. Mol. Spectrosc. 183 (1997) 1–5.
[16] T.C. Steimle, D.R. Woodward, J.M. Brown, Astrophys. J. Lett. 294 (1985) L59–L62.
[17] T.C. Steimle, D.R. Woodward, J.M. Brown, J. Chem. Phys. 85 (1986) 1276–1282.
[18] D.H. Levy, J. Hinze, Astrophys. J. 211 (1975) 980–984.
[19] P. Kristiansen, L. Veseth, J. Chem. Phys. 84 (1986) 6336–6344.
[20] T.J. Sears, P.R. Bunker, A.R.W. McKellar, K.M. Evenson, D.A. Jennings, J.M. Brown, J. Chem. Phys. 77 (1982) 5348–5362.
[21] J.M. Brown, C.M.L. Kerr, F.D. Wayne, K.M. Evenson, H.E. Radford, J. Mol. Spectrosc. 86 (1981) 544–554.
[22] J.M. Brown, E.A. Colbourn, J.K.G. Watson, F.D. Wayne, J. Mol. Spectrosc. 74 (1983) 294–318.
[23] J.M. Brown, M. Kaise, C.M.L. Kerr, D.J. Milton, Mol. Phys. 36 (1978) 553–583.
[24] J.M. Brown, J.K.G. Watson, J. Mol. Spectrosc. 65 (1977) 65–74.
[25] G. Herzberg, Spectra of Diatomic Molecules, Van Nostrand, Princeton, NJ, 1950.
[26] P.F. Bernath, C.R. Brazier, T. Olsen, R. Hailey, W.T.M.L. Fernando, C. Woods, J.L. Hardwick, J. Mol. Spectrosc. 147 (1991) 16–26.
[27] J.K.G. Watson, J. Mol. Spectrosc. 45 (1977) 99–113.
[28] J.K.G. Watson, J. Mol. Spectrosc. 80 (1980) 411–421.
[29] J.M. Brown, H. Uehara, Mol. Phys. 24 (1972) 1169–1174.
[30] R.F. Curl Jr., Mol. Phys. 9 (1965) 585–597.
[31] P. Swings, L. Rosenfeld, Astrophys. J. 86 (1937) 483–486.
[32] A. McKellar, Publ. Astron. Soc. Pac. 52 (1940) 187–192.
[33] G.J. Stacey, J.B. Lutgen, R. Genzel, Astrophys. J. 313 (1987) 859–866.
[34] J. Cernicharo, M.A. Orlandi, E. Gonzáles-Alfonso, S.J. Leeks, The Universe as seen by ISO, European Space Agency SP-427, 1999, pp. 655–658.
[35] D.M. Brink, G.R. Satchler, Angular Momentum, third ed., Oxford University Press, Oxford, 1993.
[36] D.H. Phelps, F.W. Dalby, Phys. Rev. Lett. 16 (1966) 3–4.
[37] K.I. Peterson, G.T. Fraser, W. Klemperer, Can. J. Phys. 62 (1984) 1502–1507.